Egyptian Journal of Radiology and Nuclear Medicine

RESEARCH

Open Access

Diffusion kurtosis imaging for different brain masses characterization

Reem M. Abdelnasser[1*], Aya AbdelGaleel[1], Ahmed H. Farhoud[2], Yasser Mazloum[1] and M. Ihab Reda[1]

Abstract

Background Diffusion kurtosis imaging is an advanced magnetic resonance imaging technique that reveals additional information on the microstructure and micro-dynamics of different brain masses without the need for contrast agents. The aim of this study was to provide a comprehensive analysis of the role of MRI diffusion kurtosis and to compare it with magnetic resonance spectroscopy (MRS) and dynamic susceptibility contrast perfusion (DSC) in characterizing different brain masses, including gliomas, recurrent tumors, radiation necrosis, abscesses, and infarctions. Sixty-six patients with intracranial brain masses were enrolled in this prospective study. All patients were examined by conventional MRI sequences, DSC perfusion, MRS, and diffusion kurtosis imaging, with implemented b values which were 200, 500, 1000, 1500 and 2000s/mm^2.

Results Mean kurtosis (MK) was higher ($P<0.001$) in recurrent brain tumors than in radiation-induced necrosis; the optimal MK cutoff value for differentiation between them was 642 with 91.3% sensitivity and 85.7% specificity. Mean kurtosis was also higher ($P<0.001$) in high-grade gliomas than in low-grade gliomas; the optimal MK cutoff value for differentiation between them was 639 with 91.6% sensitivity and 85.71% specificity. There was a good level of agreement between ADC and MD within the studied cases, with a correlation coefficient $r=0.815$. MK had more sensitivity and specificity in differentiation between high- and low-grade gliomas, as well as RIN and tumoral recurrence, than MRS and DSC.

Conclusions Diffusion kurtosis imaging stands as an integral, noninvasive, and noncontrast tool for the characterization of various brain masses. It augments the capabilities of traditional and advanced MRI techniques, providing a deeper understanding of the microstructural changes in brain tissues.

Keywords Diffusion kurtosis, Mean kurtosis, Contrast media, Abscess, Glioma, Magnetic resonance imaging, Infarction, Perfusion, Necrosis

Background

Diffusion kurtosis imaging has emerged as a powerful technique in neuroimaging, allowing for the assessment of microstructural alterations in brain tissue. This technique provides valuable information beyond conventional diffusion-weighted imaging by quantifying the non-Gaussian behavior of water diffusion in biological tissues. This increased interest in DKI can be attributed to its ability to detect changes in white matter regions with complex fiber arrangements, such as crossing fibers, as well as changes in isotropic structures, such as gray matter [1].

Compared to the role of standard DWI and ADC in evaluating how water molecules move outside of cells, DKI investigates non-Gaussian interactions between water molecules within tissue environments. By using more advanced mathematical curve fitting techniques and higher *b* values, mean kurtosis, another parameter

*Correspondence:
Reem M. Abdelnasser
reemahmed4122016@gmail.com
[1] Department of Radiodiagnosis, Faculty of Medicine, Alexandria University, Alexandria, Egypt
[2] Department of Neurosurgery, Faculty of Medicine, Alexandria University, Alexandria, Egypt

provided by DKI, is thought to reflect the variety and irregularity of cellular microstructure in addition to the number of interfaces found inside cell tissues [2].

Higher MK values suggest more restricted non-Gaussian diffusion, which is often seen in tumors. On the other hand, the MD value, or mean corrected apparent diffusion coefficient, represents the non-Gaussian distribution that is corrected by the average apparent diffusion coefficient. This value specifically reflects the diffusion of water molecules. By examining both MK and MD values, researchers can gain a comprehensive understanding of the diffusion characteristics within the tissue and make more accurate interpretations of tissue microstructure and pathology [3].

Adult gliomas are the most prevalent primary brain tumors, with varying degrees of malignancy. The current classification of diffuse gliomas relies on molecular analysis as the most important diagnostic criterion. Historically, gliomas were classified based solely on histological features and tumor grade. However, it is now well recognized that there can be significant heterogeneity within each grade, making accurate classification and prognostication challenging [4].

Differentiating radiation-induced necrosis from tumor recurrence can be difficult in neuroradiology since the two conditions typically exhibit similar conventional MRI findings. Accurate diagnosis of both entities is essential and will influence the treatment strategy significantly. According to recent research, DKI may be a useful method for distinguishing radiation-induced necrosis from glioma recurrence [5, 6].

Another study underscores the potential utility of DK metrics and white matter modeling in the analysis of stroke. They found that ischemia primarily affects the intra-axonal component of white matter more than it does the extra-axonal. This finding aligns with the suggested occurrence of axonal beading [7].

Aim of the study

The aim of this study was to provide a comprehensive analysis of the role of MRI diffusion kurtosis and to compare it with MRS and DSC perfusion in characterizing different brain masses, including gliomas, recurrent tumors, radiation necrosis, abscesses, and infarctions.

Methods

Patients and study design

Between May 2021 and September 2023, sixty-six patients were included in this prospective trial. All patients gave their written informed consent before participating.

Inclusion criteria

- Patients with intra-axial brain lesions on the basis of conventional MRI findings.

Exclusion criteria

Contraindication to MRI (i.e., patients with pacemakers or metallic clips).

- Patients with extra-axial brain lesions.
- Age less than 5 years old.

Flow Chart of the study is illustrated as Fig. 1.

We enrolled: (A) Thirty-seven patients who had previously undergone surgery for primary brain tumors and received postoperative chemotherapy and radiation therapy with a newly developed enhancing lesion at the operative bed. (B) Nineteen patients with newly diagnosed gliomas (12 with a high grade and 7 with a low grade). (C) Seven patients with cerebral infarctions. (D) Three patients with pyogenic abscesses.

MRI imaging protocol

- MRI examinations were obtained with a 1.5 T closed MRI scanner (Siemens, Aera, Germany) using a 8-channel head coil.The subsequent protocols were used to get MR images: (a) Conventional MRI including the pre-contrast series comprised of axial and sagittal T1-weighted spin echo (repetition time TR msec/echo time msec TE, 600/15), axial and coronal T2-weighted turbo spin echo (4000/100), and axial F LAIR (TR/TE/TI msec, 11,000/140/2200). The postcontrast series comprised 3D gradient T1 MPR sequences, axial, coronal, and sagittal T1-weighted spin echo image. (b) Functional mri including diffusion-weighted imaging (DWI) having three orthogonal directions (x, y, and z) and diffusion gradient b values of 0 and 1000 s/mm^2 with TR, 5072; number of sections is 16–22), Diffusion kurtosis: spin echo echo planar imaging DW imaging sequence was used to acquire the DK imaging data (TR = 4200, TE = 98 ms, FOV Voxel size: $0.6 \times 0.6 \times 5$ mm^3). Implemented b values were 200, 500, 1000, 1500 and 2000s/mm^2 along 30 diffusion encoding directions. MRI spectroscopy 2D multi-voxel CSI with average TE echo time (144 ms) (TR 988 ms, 180 mm FOV, acquisition time 6 min 32 s). (c) Dynamic imaging: Dynamic susceptibility-weighted contrast-enhanced gradient Echoplanar imaging (TR/TE: 1250 ms/54 ms,

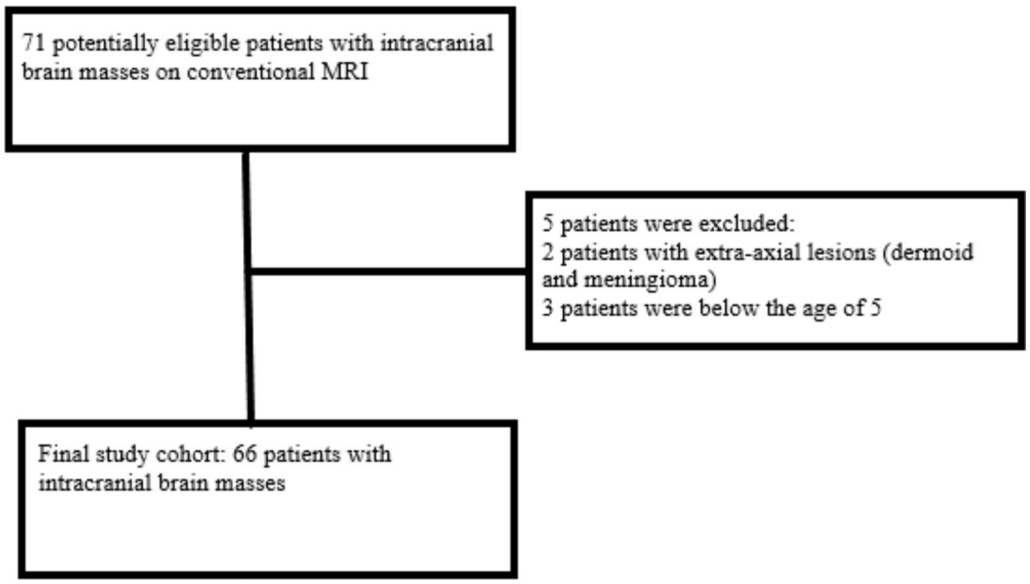

Fig. 1 Flow chart of the study population

flip angle: 35°). Before, during, and after the contrast agent bolus injection, a series of gradient-echo echo-planar pictures were obtained and T2*-weighted susceptibility signal intensity time curves and CBV maps were created.

Image data analysis and postprocessing

Using the syngo.via Frontier MR body diffusion toolbox, diffusion-weighted images were processed. The diffusion and kurtosis tensors were then computed on a voxel-by-voxel basis. The equation $S = S0 \times \exp(-b \times \mathrm{MD} + b2 \times \mathrm{MD2} \times \mathrm{MK}/6)$ was used to fit diffusion-weighted signal intensities as a function of b-value, where b denotes the b-value, MD represents corrected apparent diffusion that accounts for non-Gaussian diffusion behavior, and MK represents excessive kurtosis. Furthermore, using b values ranging from 0 to − 500 s/mm^2 based on a typical mono-exponential fit with the equation $S = S0 \times \exp(-b \times \mathrm{ADC})$, the toolbox also calculated the ADC for each pixel. Parametric maps for MK, MD, and ADC values were produced based on these computations.

Region of interest analysis (ROI)

- Regions of interest across multiple slices were manually drawn around the enhancing component of the lesion, and in nonenhancing lesions, the ROI was drawn around the restricted part with the lowest ADC value. The size of the ROI was variable depending on the area of restriction or enhancement with the average range from 20 to 80 mm^2.
- Regions of interest were placed by two experienced radiologists with 30 and 5 years of experience in neuroradiology, and they assessed the DKI maps simultaneously in a single-joined setting, reaching a consensus.

Perfusion and spectroscopy

- On a voxel-by-voxel basis, CBV maps were computed and displayed as an overlay image with the contrast T1-weighted images after T2*-weighted signal intensity time curves were generated. The rCBV cutoff value for differentiation between high- and low-grade gliomas as well as tumoral recurrence and radiation-induced necrosis was 1.75 and 1.3, respectively [8, 9].
- A point-resolved spectroscopic sequence (PRESS) with 2000/144 ms [TR/TE] that comprised water and outer volume saturation pulses. On contrast-enhanced axial T1-weighted images, the volume of interest (VOI) was positioned to match the contrast-enhancing region. The following metabolite peaks were used: lipid-containing compounds (Lip) in the range of 0.9–1.3 ppm, lactate (Lac) at 1.33 ppm (inverted β-methyl doublet), choline (Cho) at 3.22 ppm, (phospho-) creatine (Cr) at 3.02 ppm, and N-acetylaspartate (NAA) at 2.02 ppm. The metabolite ratios (NAA/Cr, Cho/Cr, Cho/NAA, and NAA/Cho). The cutoff values for Cho/Cr were 2 for differentiation between both high- and low-grade

gliomas as well as tumoral recurrence and radiation-induced necrosis, while Cho/NAA was 2 and 1.8, respectively [10, 11].

The final diagnosis

- The definitive diagnosis of brain lesions was determined through histopathology, or MRI examinations every three months for six to twelve months. High-grade gliomas and four low-grade gliomas were confirmed by histopathology, while three low-grade gliomas were confirmed through serial follow-up. One abscess case was surgically drained; the others were on serial follow-up.
- Using the RANO criteria for response assessment in neuro-oncology, a tumoral recurrence was determined whether the lesion's size increased by at least 25%. Radiation necrosis was identified if no size, shrinkage, or complete disappearance occurred over six months or more. Most postoperative cases were confirmed by follow-up, with only three cases reopened surgically: two confirmed as recurrence and the other one as radiation-induced necrosis [12].
- Ischemic lesions were diagnosed based on clinical symptoms, territorial distribution and follow-up (7 cases).

Statistical analysis

Data were fed to the computer and analyzed using IBM SPSS (Statistical Package for the Social Sciences) software package version 20.0. (Armonk, NY: IBM Corp). Categorical data were represented as numbers and percentages. For continuous data, quantitative data were expressed as range (minimum and maximum), mean, standard deviation and median for normally distributed quantitative variables. Student t-test was used to compare two groups. Pearson coefficient, Bland–Altman plot and intraclass correlation coefficient for agreement between ADC and MD was used and receiver operating characteristic curve (ROC) was used to determine the diagnostic performance of the markers and cutoff values, area more than 50% gives acceptable performance and area about 100% is the best performance for the test. The significance of the obtained results was judged at the 5% level.

Results

Sixty-six patients with intracranial brain masses on the basis of conventional radiologic findings were enrolled in this prospective study (25 women and 41 men; age range, 6–70 years; mean age, 45.49 ± 15.01 years) (Table 1).

Table 1 Distribution of the studied cases according to demographic data ($n=66$)

	No. (%)
Sex	
Male	41 (62.12%)
Female	25 (37.87%)
Total	66
Age (/years)	
Mean ± SD	45.49 ± 15.01
Median (Min.–Max.)	46 (6–73)

SD standard deviation

Table 2 Descriptive analysis of the studied cases according to MK in each lesion ($n=66$)

	No	MK Mean ± SD
Low-grade glioma	7	412.1 ± 148.6
High-grade glioma	12	906.0 ± 183.2
Abscess	3	1327.0 ± 467.3
Acute infarct	5	1428.4 ± 397.3
Chronic infarct	2	404.5 ± 119.5
Recurrence	23	873. 3 ± 215.6
RIN	14	418.6 ± 238.5

Of the sixty-six patients, 12 (18%) were diagnosed with high-grade gliomas (grades III and IV) and 7 (10.6%) were diagnosed with low-grade gliomas (grades I and II). Patients with history of tumoral excision: 23 (34.8%) patients were diagnosed with tumoral recurrence and 14 (21.2%) patients with RIN. Other patients: 5 (7.5%) patients were diagnosed with acute ischemic infarctions, 2 (3%) with chronic ischemic infarcts, and 3 (4.5%) with pyogenic abscesses.

The mean kurtosis values for the lesions are shown in (Table 2), showing the highest values are within the acute ischemic infarcts as well as the abscesses (Figs. 2, 3) and the lowest values within the chronic ischemic infarcts, low-grade gliomas, and RIN.

Mean kurtosis values were higher ($P<0.001$) in recurrent brain tumors than in radiation-induced necrosis; the optimal MK cutoff value for differentiation between them was 642 with 91.3% sensitivity, 85.7% specificity, and 89.18% accuracy. Also, mean diffusion (MD) was lower ($P<0.024$) in recurrent brain tumors than in radiation-induced necrosis; the optimal MD cutoff value for differentiation between them was $1.73\times10^{-3}mm^2/sec$ with 78.2% sensitivity, 57.1% specificity, and 70.27% accuracy (Figs. 4, 5, 6) (Table 3).

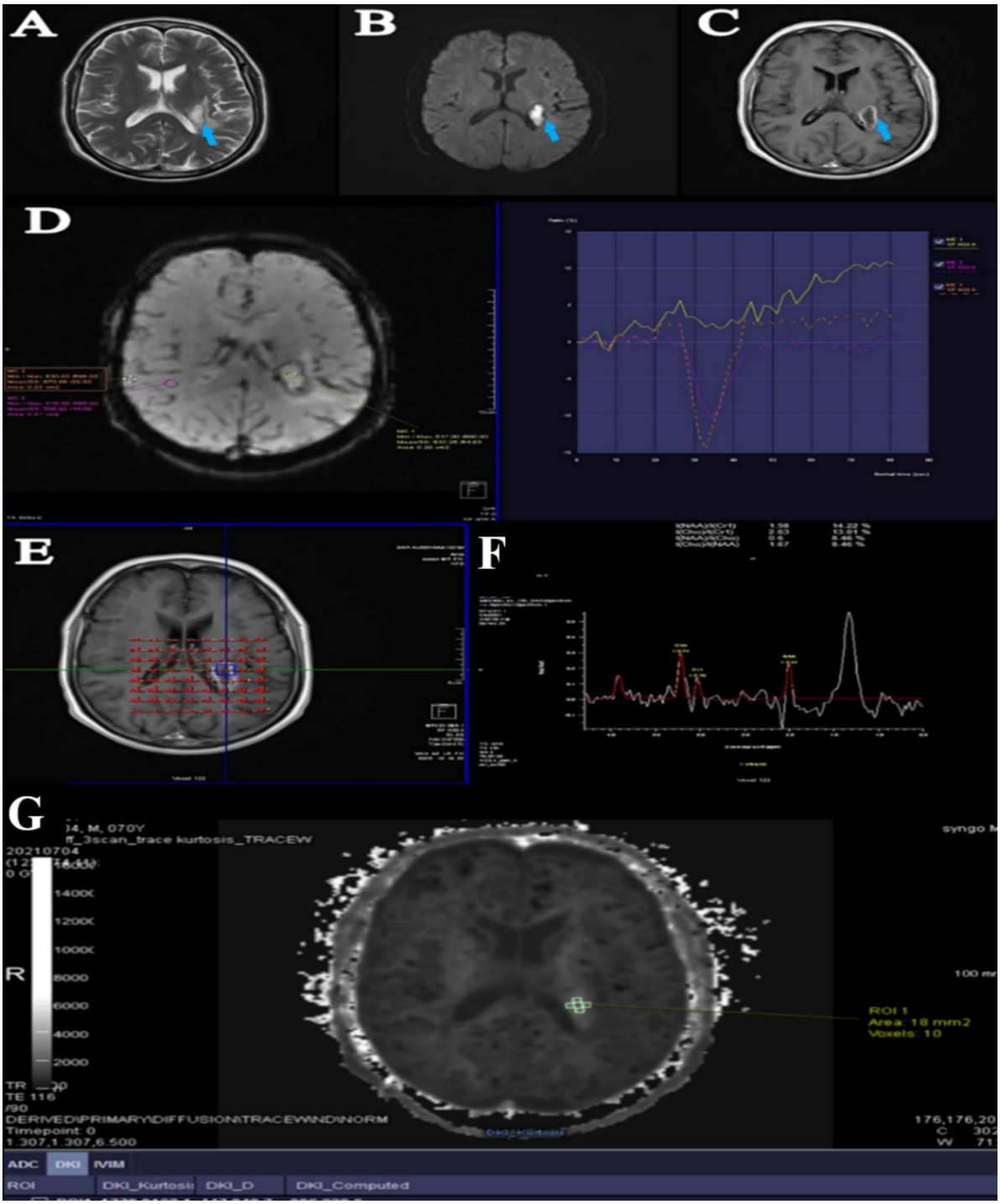

Fig. 2 A 70-year-old female patient with sudden onset of fever and disturbed level of consciousness. MRI showed; **A** Axial T2WI shows a well-defined hyperintense lesion at the left periventricular area surrounded by edema. **B** Axial DWI shows central restricted diffusion. **C** Axial T1 postcontrast shows peripheral rim of enhancement. **D** T2* signal intensity time curve shows that the lesion is hypo-perfused in comparison to the contralateral normal-appearing white matter (NAWM) with rCBV measuring 0.79 (lesion: solid yellow line, contralateral NAWM: purple dashed line). **E** and **F** MRS showing a non-neoplastic curve (Cho/Cr = 2.6 and Cho/NAA = 1.6 with a high lipid peak. **G** Diffusion kurtosis image showing high mean kurtosis = 1866. Features suggesting left periventricular abscess

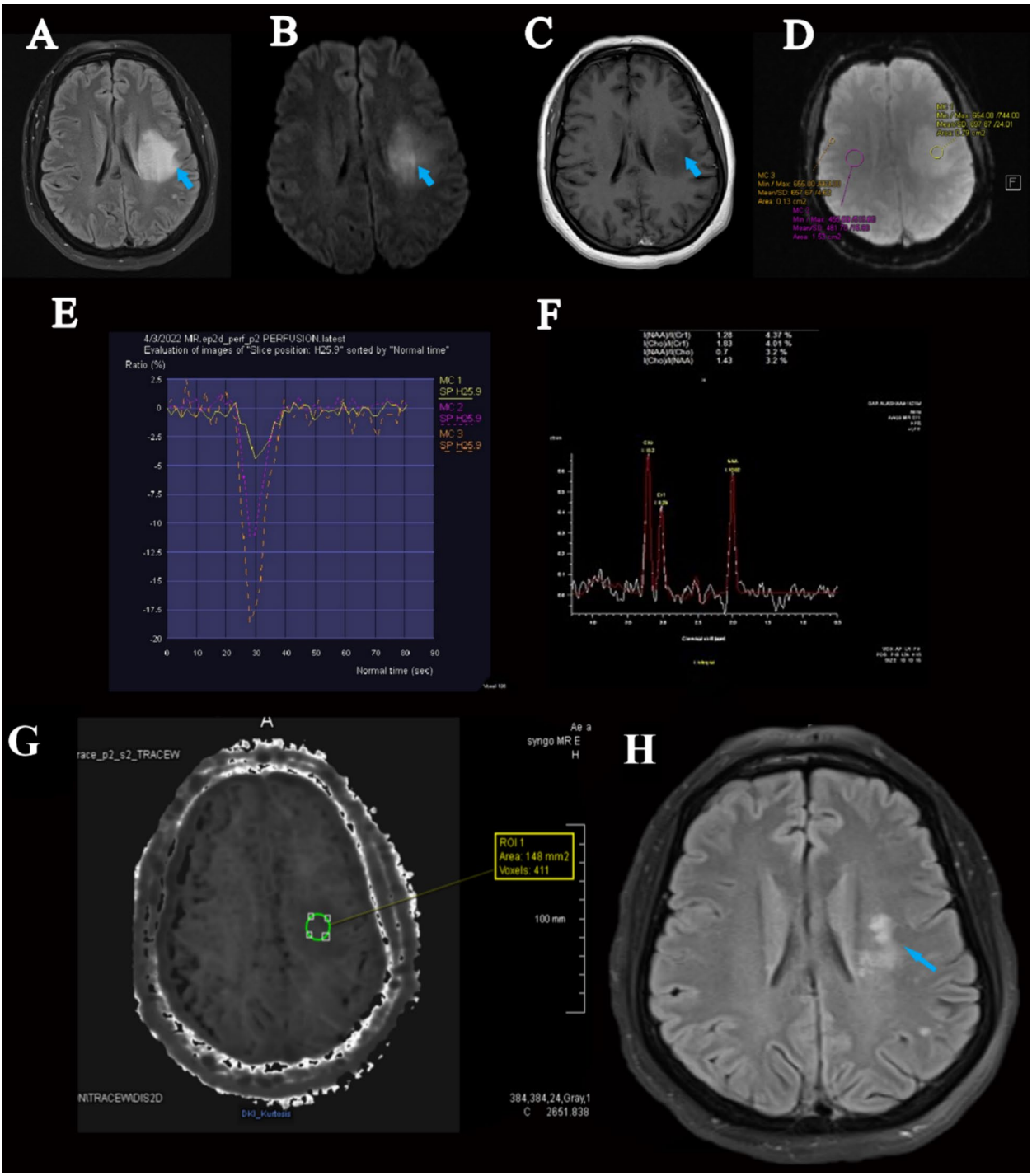

Fig. 3 A 66-year-old female patient with sudden onset of right lag. MRI showed; **A** Axial FLAIR shows hyperintense area at the left corona radiate. **B** Axial DWI showed restricted diffusion. **C** Axial T1 postcontrast showing no enhancement. **D** and **E** T2* signal intensity time curve shows the lesion is hypo-perfused in comparison to the contralateral NAWM with rCBV measuring 0.65 (lesion: solid yellow line, contralateral NAWM: purple dashed line). **F** MRS showing a non-neoplastic curve (Cho/Cr = 1.83 and Cho/NAA = 1.43 with presence of lactate and lipid peaks). **G** Diffusion kurtosis image showing high mean MK = 1110. **H** Follow-up after 3 months showing regression in the size of the lesion in axial FLAIR image. Features matching with acute infarction along the left middle cerebral artery territory. Final diagnosis was reached based on clinical picture and imaging findings

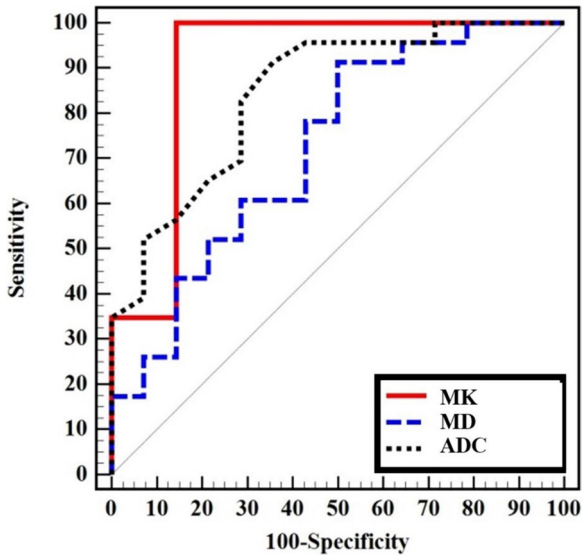

Fig. 4 ROC curve for MK lesion, MD and ADC to discriminate recurrence ($n=23$) from RIN ($n=14$)

Mean kurtosis values were higher ($P<0.001$) in high-grade gliomas than in low-grade gliomas; the optimal MK cutoff value for differentiation between them was 639, with 91.6% sensitivity, 85.71% specificity, and 89.47% accuracy. Also, MD was lower ($P<0.011$) in high-grade gliomas than low-grade gliomas; the optimal MD cutoff value for differentiation between them was 1.36×10^{-3}mm^2/sec with 83.3% sensitivity, 85.7% specificity, and 84.21% accuracy (Table 4) (Figs. 7, 8).

There was a good level of agreement between ADC and MD within the studied cases, with a correlation coefficient of 0.815 (Table 5) (Fig. 9).

MRS and DCS perfusion showed 95.65% sensitivity, 92.86% specificity, and 94.59% accuracy in differentiation between RIN and tumoral recurrence cases compared to 100% sensitivity, 85.71% specificity, and 94.59% accuracy of MK in these cases. The final diagnosis was reached by follow-up or biopsy (Table 6).

MRS and DCS perfusion showed 91.67% sensitivity, 57.14% specificity, and 78.95% accuracy in differentiation between RIN and tumoral recurrence cases, compared to 100% sensitivity, 85.71% specificity, and 94.74% accuracy of MK in these cases. The final diagnosis of most of these lesions was by biopsy (Table 7) (Figs. 10, 11).

One case of tumoral recurrence was diagnosed falsely as RIN by advanced techniques (mainly perfusion) while being correctly diagnosed as recurrence by DKI (Fig. 12).

Discussion

Diffusion kurtosis imaging is a technique used to evaluate the microstructural changes in the brain. It provides information about the diffusion of water molecules in the brain, specifically focusing on non-Gaussian diffusion. This non-Gaussian diffusion is a result of the presence of barriers and compartments within the brain tissue. These barriers and compartments can alter the diffusion of water molecules, and quantifying the degree of non-Gaussianity can provide valuable insights into brain pathologies such as brain tumors, ischemic stroke, Alzheimer's disease, and schizophrenia [13].

The aim of this study was to investigate if DKI characteristics, which do not require intravenous contrast, may be a suitable alternative to MRS and DSC for the accurate evaluation of different brain masses and to compare these modalities.

One of the most common brain masses that require adequate assessment is brain gliomas. The grading system for astrocytomas developed by the World Health Organization evaluates factors such as necrosis, vascular proliferation, tumor cellularity, and mitosis. The heterogeneity of these tumors leads to substantial variations in treatment and prognosis depending on the pathologic grade. The complexity further increases as individual tumors usually exhibit heterogeneity, with the final pathologic grade determined by the most aggressive traits in a region [14].

Extensive efforts have been dedicated to differentiating high-grade and low-grade gliomas before surgery and pinpointing regions requiring biopsy or resection based on their suspicious appearance. Much consideration has been given to attributes such as the pattern of enhancement, perfusion data, and parameters of diffusion tensor imaging of the lesions. However, diffusion kurtosis imaging permits the identification of microstructural differences within and between gliomas by providing an extra imaging biomarker [15].

In our study, we depended on MK values for differentiation between low- and high-grade gliomas. MK was higher in high-grade than low-grade gliomas, with cutoff value of 639 with 91.6% sensitivity and 85.71% specificity. These results agreed with a study conducted by Van Cauter et al. [16], as they compared various diffusion imaging parameters such as the mean diffusivity, fractional anisotropy, mean kurtosis, radial kurtosis, and axial kurtosis among 28 brain tumor patients. Their findings demonstrated significant differences in kurtosis parameters between high-grade and low-grade gliomas. High-grade tumors exhibited higher kurtosis values, which could be attributed to increased cell density, reduced cell size, and a more complex intracellular environment. They concluded

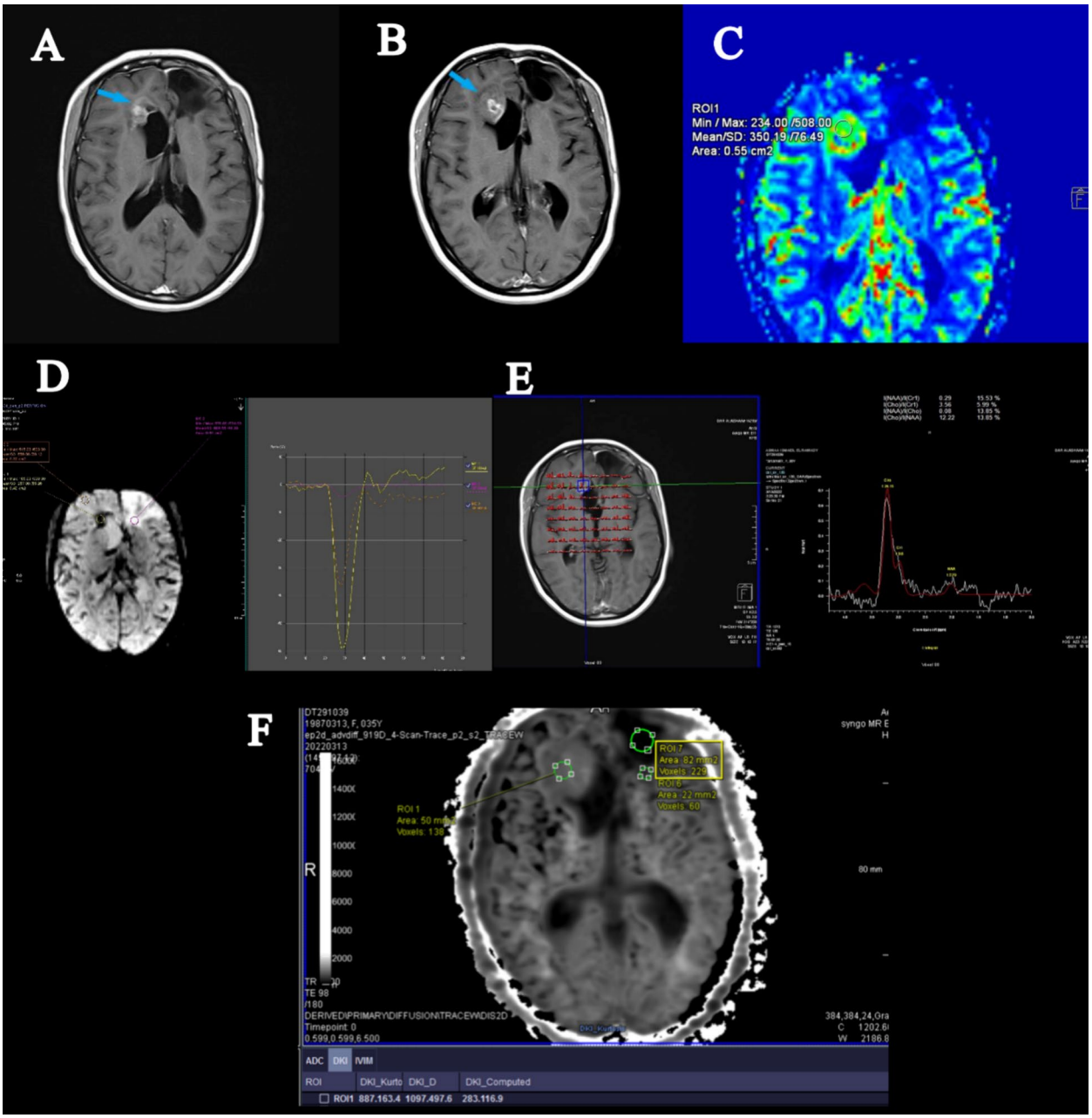

Fig. 5 A routine follow-up MRI of a 35-year-old female patient who had a history of chemotherapy and radiation after a surgical removal of a left frontal oligodendroglioma revealed; **A** Axial T1 post-GAD showing heterogeneously enhancing lesion at right frontal periventricular zone with postoperative left frontal encephalomalacic area. **B** The lesion progressed in size at the 6-month follow-up. **C** and **D** CBV color map and T2* signal intensity time curve shows the lesion is hyper-perfused in comparison to the contralateral NAWM with rCBV measuring 6.6 (lesion: solid yellow line, contralateral NAWM: purple dashed line). **E** MRS showing a neoplastic curve (Cho/Cr = 12.2 and Cho/NAA = 3.5). **F** Diffusion kurtosis image showing high MK = 887 suggesting tumoral recurrence

(See figure on next page.)

Fig. 6 A regular follow-up MRI of a 60-year-old male patient, who had surgery to remove a left frontal GBM and received chemotherapy and radiotherapy revealed; **A** Axial T1 post-GAD showing linear enhancing lesion at operative bed. **B** DWI showing free diffusion. **C** and **D** The lesion is hypo-perfused in comparison to the contralateral NAWM with rCBV measuring 1.25 (lesion: solid red line, contralateral NAWM: yellow dashed line) as indicated by the T2* signal intensity time curve. **E** MRS showing a non-neoplastic curve (Cho/Cr = 1.06 and Cho/NAA = 1.44) and prescence of lactate peak. **F** Diffusion kurtosis image showing low mean MK = 305 suggesting RIN at the operative bed

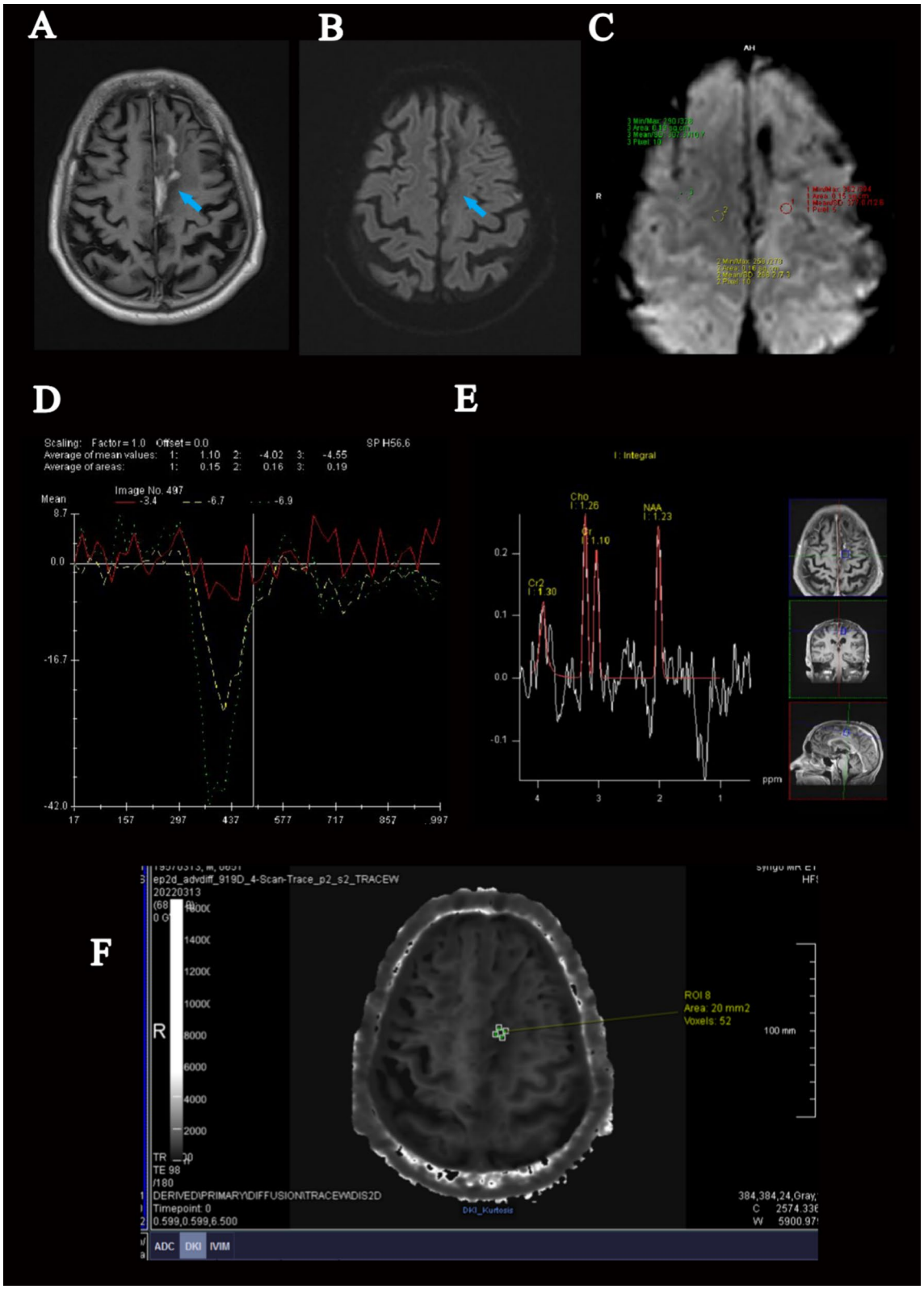

Fig. 6 (See legend on previous page.)

Table 3 Diagnostic performance for MK, MD and ADC to discriminate recurrence ($n=23$) from RIN ($n=14$)

	AUC	*p*	95% CI	Cutoff	Sensitivity (%)	Specificity (%)	PPV (%)	NPV (%)	Accuracy (%)
MK	0.907*	< 0.001*	0.783–1.000	> 642	91.30	85.71	91.3	85.7	89.18
MD ($\times 10^{-3}$ mm^2/sec)	0.724*	0.024*	0.550–0.897	≤ 1.735	78.26	57.14	75.0	61.5	70.27
ADC ($\times 10^{-3}$ mm^2/sec)	0.845*	0.001*	0.715–0.975	≤ 1.1[#]	91.3	64.29	80.8	81.8	81.08

AUC area under a curve, *p value* probability value, *CI* confidence intervals, *NPV* negative predictive value, *PPV* positive predictive value

*Statistically significant at $p \leq 0.05$, [#]Cutoff was choose according to Youden index

Table 4 Diagnostic performance for MK, MD and ADC to discriminate high-grade glioma ($n=12$) from low-grade glioma ($n=7$)

	AUC	*p*	95% CI	Cutoff	Sensitivity (%)	Specificity (%)	PPV (%)	NPV (%)	Accuracy (%)
MK	0.988	0.001*	0.951–1.000	> 639	91.67	85.71	91.7	85.7	89.47
MD ($\times 10^{-3}$ mm^2/sec)	0.857	0.011*	0.674–1.000	≤ 1.364[#]	83.33	85.71	90.9	75.0	84.21
ADC ($\times 10^{-3}$ mm^2/sec)	0.982	0.001*	0.934–1.000	≤ 0.9	91.67	85.71	91.7	85.7	89.47

AUC area under a curve, *p value* probability value, *CI* confidence intervals, *NPV* NEGATIVE predictive value, *PPV* positive predictive value

*Statistically significant at $p \leq 0.05$, [#]Cutoff was choose according to Youden index

that kurtosis parameters provided a better distinction between the two types of gliomas compared to traditional diffusion imaging parameters. It was possible to distinguish between low- and high-grade lesions with the highest sensitivity and specificity (100% and 73%, respectively) when the mean kurtosis was normalized to the value in the contralateral normal-appearing white matter.

Also, in a separate study conducted by Raab et al. [17], they distinguished between low- and high-grade gliomas according to their diffusion patterns, which agreed with us. In higher-grade gliomas, they saw an increase in MK levels. Compared to both the apparent diffusion coefficient and FA, normalized MK offered a clearer difference between low- and high-grade cancers.

Postmanagement tumor recurrence and radiation-induced necrosis are additional relevant brain masses for distinction. The clinical indicators and conventional MRI findings, including enhanced tissues at the surgical site, are comparable, yet they require completely distinct treatment modalities. Accurate diagnosis of these conditions still relies heavily on stereotactic biopsy, which is considered the definitive method. However, this method has potential drawbacks, including the risk of morbidity and the possibility of a sampling error if the removed specimen does not include tumor cell clusters. This has encouraged the search for an accurate, noninvasive alternative to surgery. Previous attempts have employed MR spectroscopy and positron emission tomography to differentiate between tumor recurrence and radiation necrosis, but results have been inconsistent and often unsatisfactory, especially with histologically heterogeneous lesions that demonstrate a mix of recurrence and radiation necrosis [18].

Our results found that MK was higher ($P<0.001$) in recurrent brain tumors than in radiation-induced necrosis; the optimal cutoff value for differentiation between them was 642 with 91.3% sensitivity and 85.7% specificity.

These findings agreed with Wu et al. [6]; they observed that in the case of high-grade glioma recurrence, there was a noticeable increase in relative mean kurtosis (rMK) and a decline in the relative mean diffusivity (rMD) within the enhancing lesions, which contrasted with pseudo-progression (PsP) cases ($P<0.001$ and $P=0.006$, respectively). In conclusion, diffusion kurtosis imaging showed superior capability in distinguishing between high-grade glioma recurrence and PsP, with rMK serving as the best independent predictive factor.

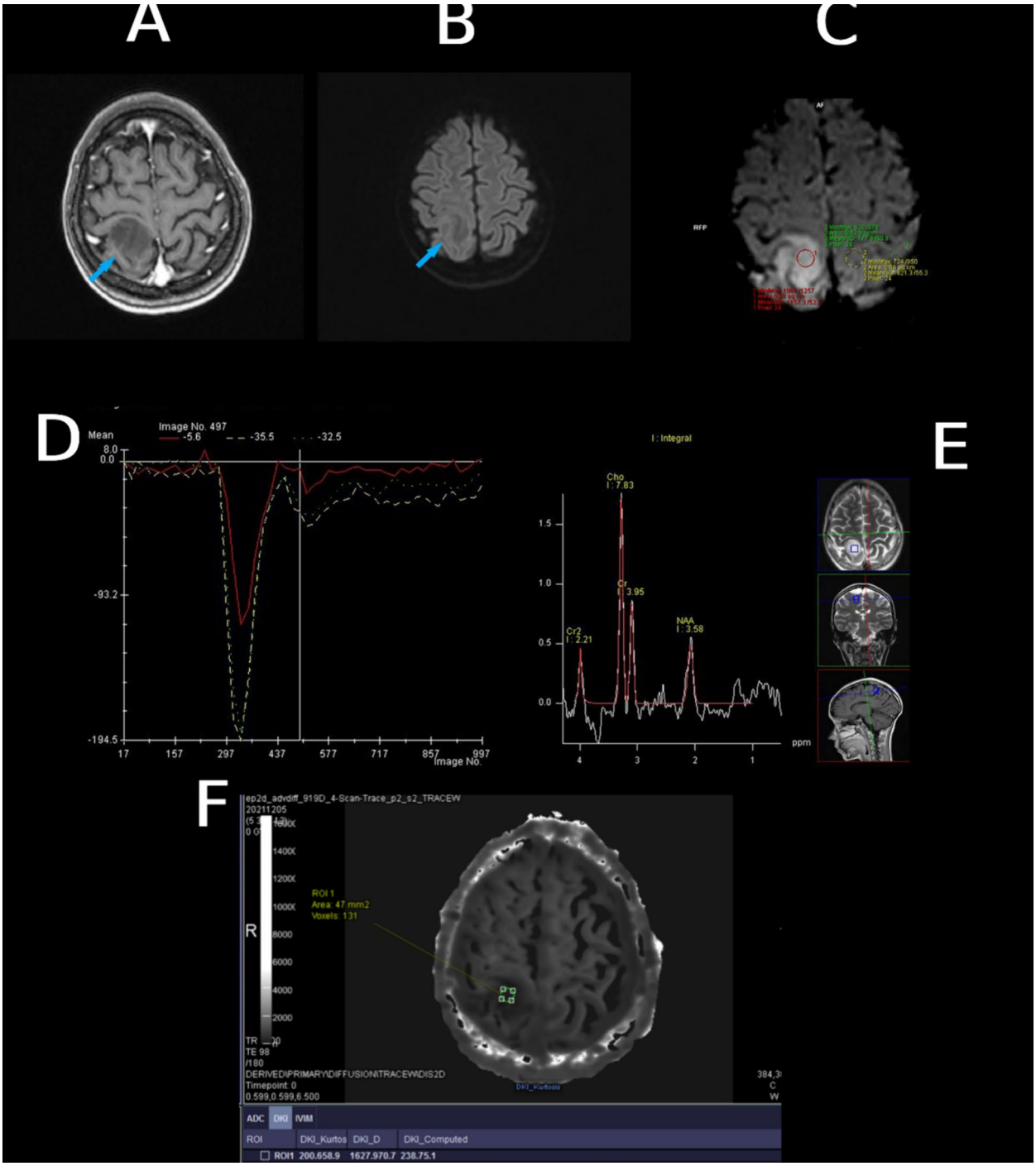

Fig. 7 A 32-year-old female patient presenting with a newly diagnosed glioma. **A** Axial T1 post-GAD showing a well circumscribed right parietal lesion showing no enhancement. **B** Axial DWI showing free diffusion. **C** and **D** T2* signal intensity time curve shows the lesion is hypo-perfused in comparison to the contralateral NAWM with rCBV measuring 2.35 (lesion: solid red line, contralateral NAWM: yellow dashed line). **E** MRS showing a neoplastic curve (Cho/Cr = 1.98 and Cho/NAA = 2). **F** Diffusion kurtosis image showing low mean MK = 200 indicating low-grade glioma

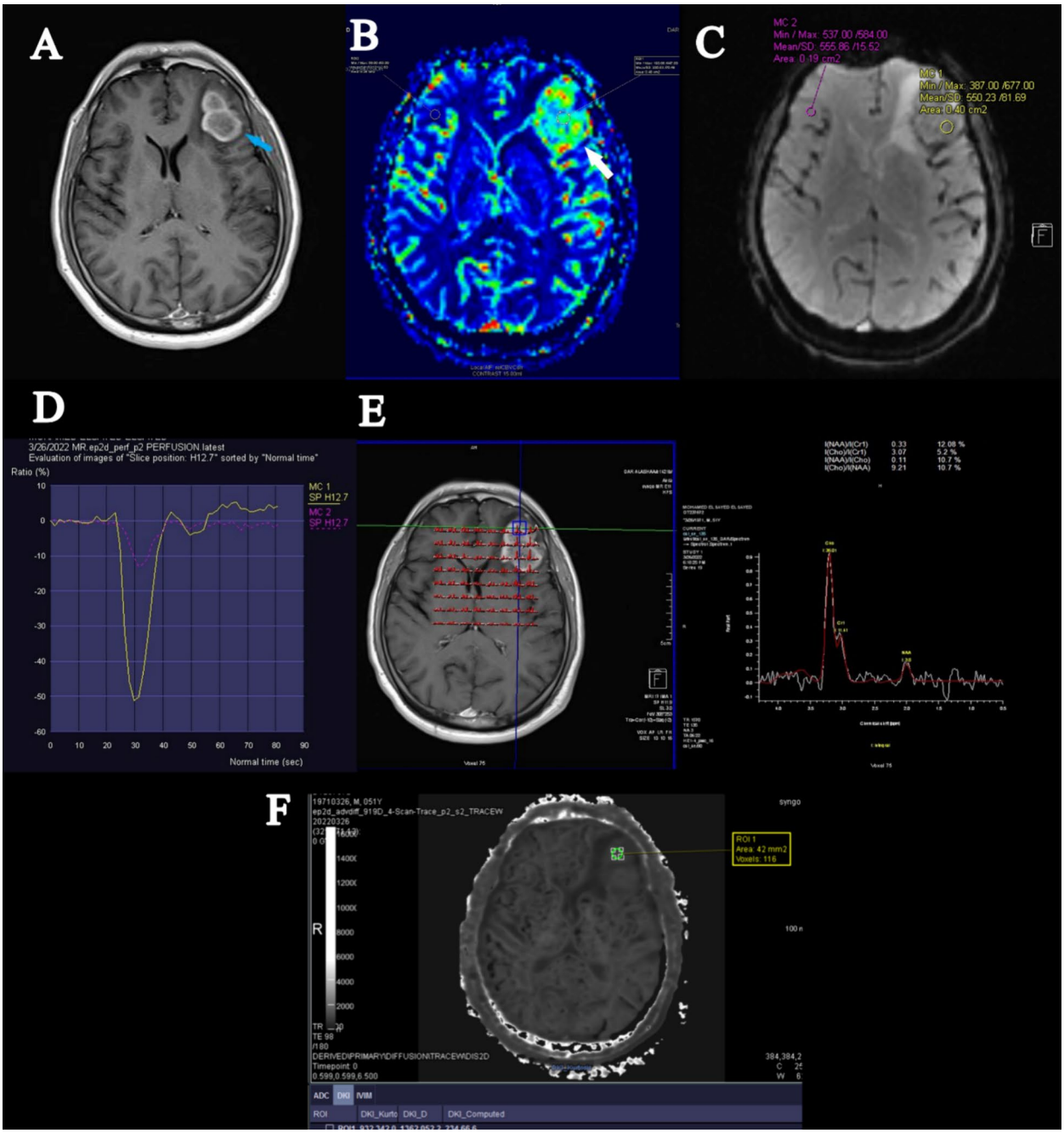

Fig. 8 A 66-year-old male patient presenting with a newly diagnosed glioma. **A** Axial T1 post-GAD showing a lobulated left frontal lesion showing heterogenous postcontrast enhancement. **B** CBV color map: the lesion is hyper-perfused with rCBV measuring 5.8. **C** and **D** T2* signal intensity time curve shows the lesion is hyper-perfused in comparison to the contralateral NAWM (lesion: solid yellow line, contralateral NAWM: purple dashed line). **E** MRS showing a neoplastic curve (Cho/Cr = 3 and Cho/NAA = 9.2). **F** Diffusion kurtosis image showing high mean MK = 932 suggesting high-grade glioma

Table 5 Agreement between ADC and MD in the studied cases ($n=66$)

	ADC ($\times 10^{-3}$ mm^2/sec)	MD ($\times 10^{-3}$ mm^2/sec)
Mean ± SD	0.96 ± 0.43	1.43 ± 0.64
Median (Min.–Max.)	0.82 (0.30–2.20)	1.25 (0.46–3.43)
Difference	0.468 ± 0.330	
Correlation coefficient		
r (*p*)	0.883* (< 0.001*)	
Intraclass correlation coefficient		
P	< 0.001*	
ICC (LL–UL 95%C.I)	0.815 (0.715–0.883)	
Level of agreement	Good agreement	

r Pearson coefficient, *ICC* intraclass correlation coefficient, *CI* confidence interval, *LL* lower limit, *UL* upper limit, *p*: *p* value for comparing between ADC and MD

*Statistically significant at $p \leq 0.05$

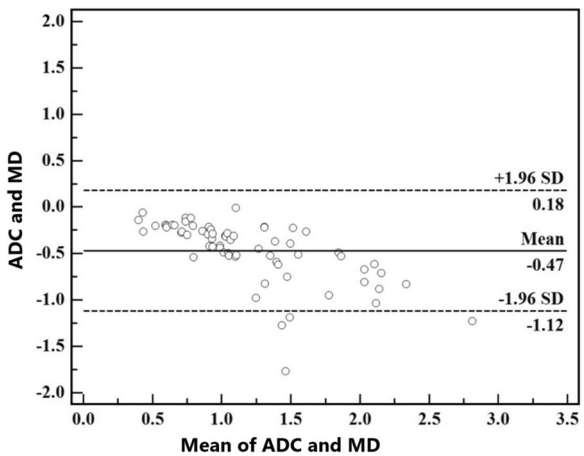

Fig. 9 Bland Altman for ADC and MD in the studied cases ($n=66$)

Shi et al. [19], also coupled diffusion kurtosis and dynamic susceptibility contrast-enhanced MRI in another study to distinguish between pseudo-progression and high-grade glioma recurrence. They found the rMK, relative axial kurtosis (rKa), relative cerebral blood volume (rCBV), and relative mean transit time (rMTT) for glioma recurrence were higher than those seen in pseudo-progression; all changes were statistically significant ($P<0.05$). The combined application of rMK and rCBV boosted the AUC to 0.924 ($P<0.001$) and increased the diagnostic accuracy to 88.24%; these results reinforced ours.

Table 6 Sensitivity, specificity, and accuracy for advanced imaging techniques (MRS and DSC) and MK in differentiation between RIN and Recurrence

	Diagnosis		Sensitivity (%)	Specificity (%)	PPV (%)	NPV (%)	Accuracy (%)
	RIN ($n=14$)	Recurrence ($n=23$)					
	No	No					
Advanced imaging							
RIN	13	1	95.65	92.86	95.65	92.86	94.59
Recurrence	1	22					
MK							
RIN	12	0	100.0	85.71	92.0	100.0	94.59
Recurrence	2	23					

p: *p* value for association between different categories, *PPV* positive predictive value, *NPV* negative predictive value

Statistically significant at $p \leq 0.05$

Table 7 Sensitivity, specificity and accuracy for advanced imaging techniques (MRS and DSC) and MK in differentiation between high- and low-grade gliomas

	Diagnosis		Sensitivity (%)	Specificity (%)	PPV (%)	NPV (%)	Accuracy (%)
	Low-grade glioma (*n* = 7)	High-grade glioma (*n* = 12)					
	No	No					
Advanced							
Low	4	1	91.67	57.14	78.57	80.0	78.95
High	3	11					
MK							
Low	6	0	100.0	85.71	92.31	100.0	94.74
High	1	12					

p: *p* value for association between different categories, *PPV* positive predictive value, *NPV* negative predictive value

Statistically significant at $p \leq 0.05$

We are one of the few studies that integrated DSC perfusion and MR spectroscopy with MK for glioma grading and differentiation between RIN and tumoral recurrence. MRS and DCS perfusion showed less sensitivity and specificity than MK for both glioma grading and differentiation between RIN and tumoral recurrence. Two cases presented earlier were diagnosed as high-grade gliomas by MRS and DSC, but DK parameters were with low-grade values which were proven by biopsy to be low grade.

Van Cauter et al. [20], also found statistically significant differences among tumor grades between MK, MD, mean rCBV, lipids over total choline, lipids over creatine, sum of myo-inositol, and sum of creatine, but they stated DSC-MRI to be the modality with the best performance when comparing modalities individually, which was different from what we found.

Regarding the acute ischemic lesions, they had the highest MK value about 1428.4 ± 397.3 while the chronic ischemic lesions had the lowest MK value, 404.5 ± 119.5. These findings were in agreement with Hui et al.; their results stated higher MK values within the ischemic core than the contralateral white matter and gray matter [7].

The last lesions included in our study were pyogenic abscesses; the MK within them was also high (1327.0 ± 467.3) near that of acute ischemic insults yet higher than high-grade gliomas. This high Mk is an indicator of tissue heterogeneity within the core of the abscess. We are almost the only study to measure DK parameters within pyogenic abscesses.

This study's limitations encompass a restricted number of lesions examined and an absence of histopathological diagnosis for some of the cases. Consequently, clinical and imaging follow-up data were employed as replacement markers to infer the final diagnosis. Monitoring these lesions over time would reduce potential misclassification risks.

Conclusions

- This study demonstrated substantial variations in kurtosis parameters between high- and low-grade gliomas, as well as in recurrent gliomas and RIN; hence better separation was obtained than conventional MRI imaging.
- Diffusion kurtosis is recommended as a supplemental method to conventional MRI as a noninvasive method to evaluate various brain lesions with higher sensitivity in differentiation of the brain gliomas and tumoral recurrence than MRS and DSC

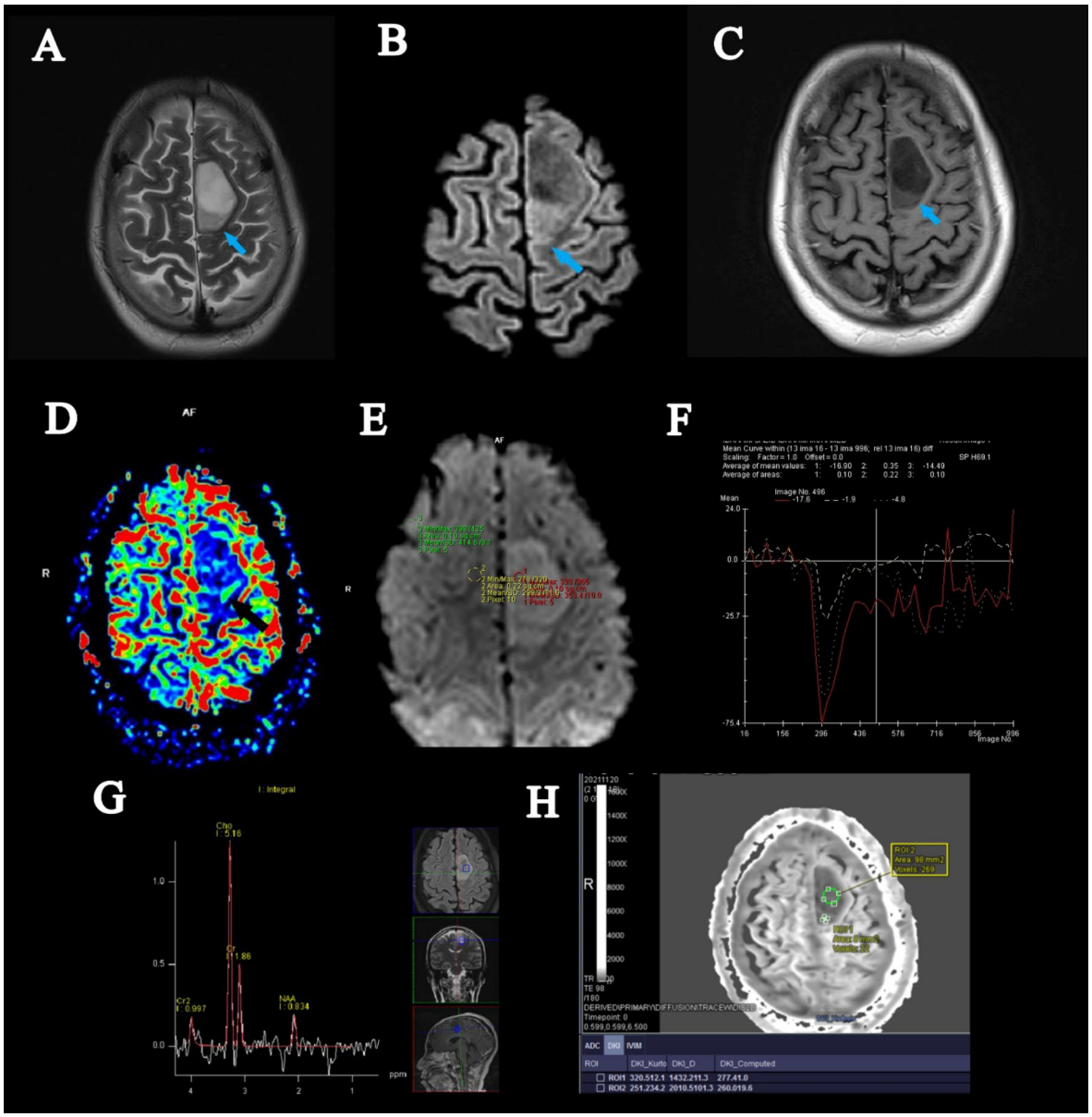

Fig. 10 A 35-year-old male patient presenting with a newly diagnosed glioma. **A** Axial T2 shows a well circumscribed left frontal lesion. **B** Axial DWI showing restricted diffusion in its posterior aspect. **C** T1 post-GAD showing no enhancement. **D** rCBV map shows areas of hyper perfusion with rCBV measuring 2.5. **E** and **F** T2* signal intensity time curve shows the lesion is hyper-perfused in comparison to the contralateral NAWM (lesion: solid red line, contralateral NAWM: yellow dashed line). **G** MRS showing a neoplastic curve (Cho/Cr = 2.77 and Cho/NAA = 6.2) matching with a high-grade glioma. **H** Diffusion kurtosis image showing low mean MK = 320 suggesting low-grade glioma. This is one of the cases that there was discrepancy between the advanced imaging (MRS and DSC) and DK, the final diagnosis was reached by biopsy and confirmed the findings of DK

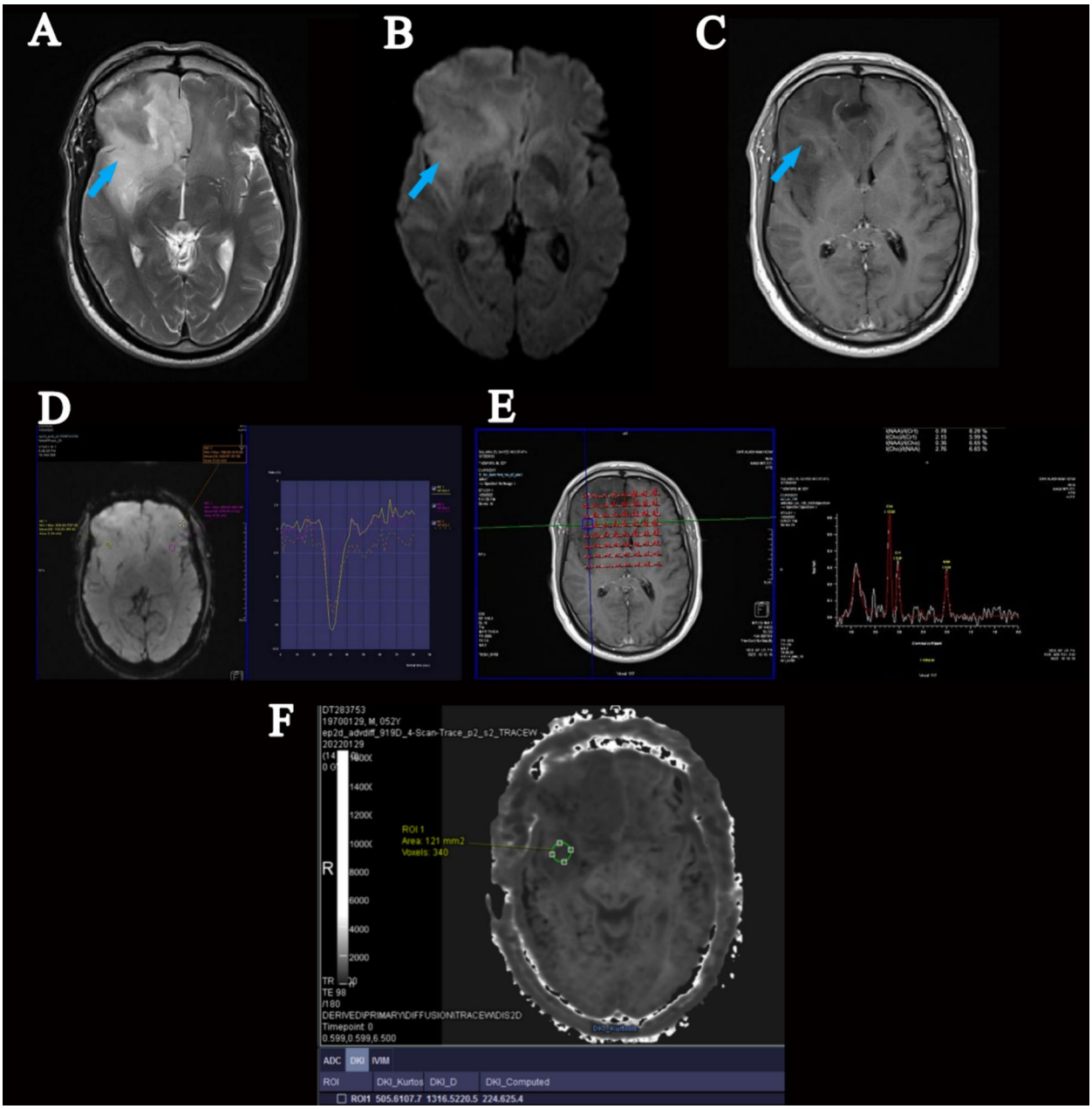

Fig. 11 A 45-year-old male patient presenting with a newly diagnosed glioma. **A** Axial T2 showing an ill-defined right frontal lesion surrounded by vasogenic edema. **B** Axial DWI showing areas of diffusion restriction. **C** T1 post-GAD showing small foci of postcontrast enhancement. **D** T2*-signal intensity time curve shows the lesion is hyper-perfused to the contralateral NAWM with rCBV measuring 3.6 (lesion: solid yellow line, contralateral NAWM: purple dashed line). **E** MRS showing a neoplastic curve (Cho/Cr = 2.77 and Cho/NAA = 6.2) matching with a high-grade glioma. **F** Diffusion kurtosis image showing low mean MK = 505 suggesting low-grade glioma. This is another case with discrepancy between the advanced imaging (MRS and DSC) and MK, the final diagnosis was reached by biopsy and confirmed the findings of DK

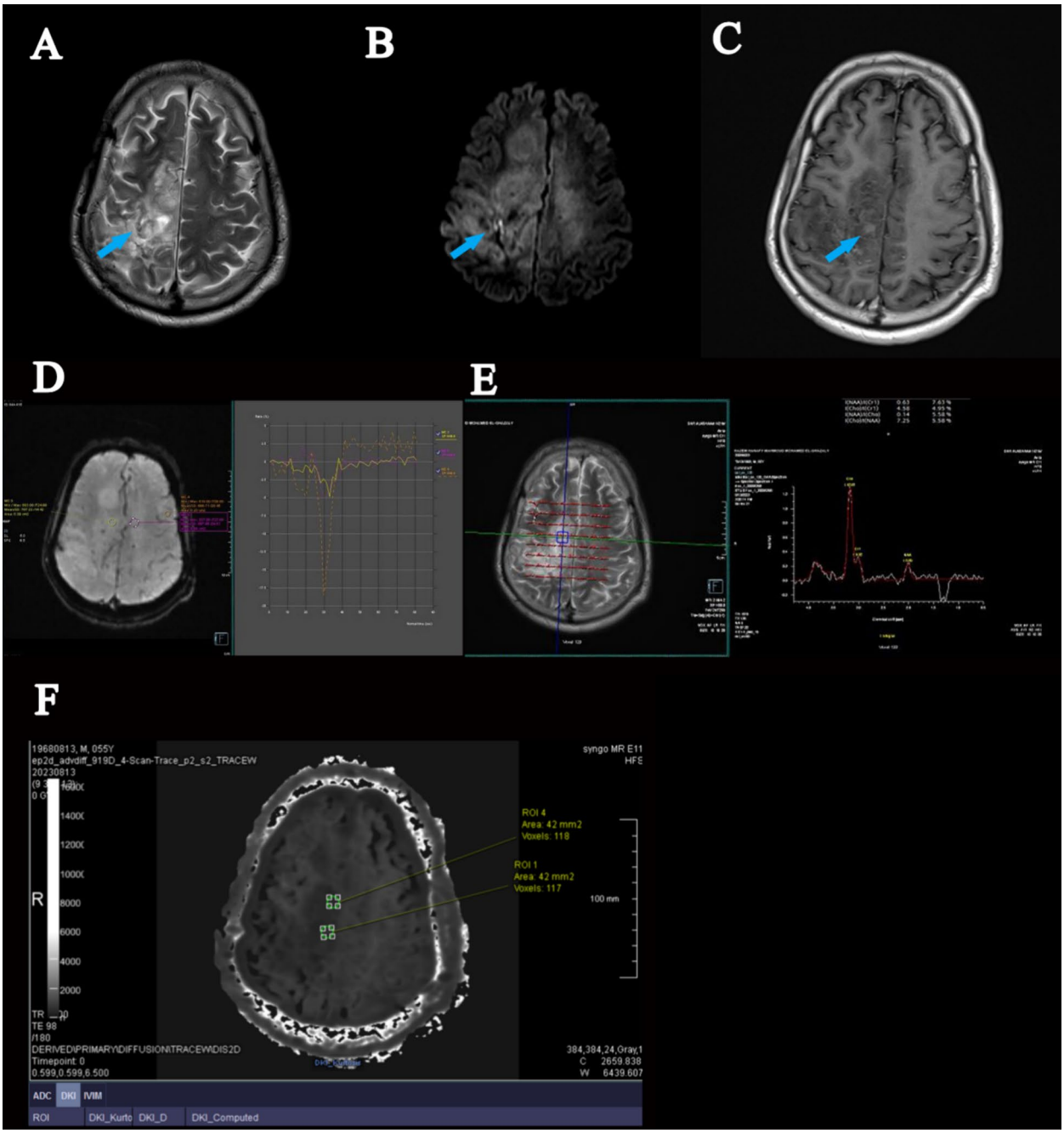

Fig. 12 A 68-year-old male patient with history of surgically removed right fronto-parietal wild type glioblastoma grade 4 followed by chemo and radiotherapy; routine follow-up MRI showed; **A** Axial T2 showing ill-defined mass lesion at the operative bed. **B** Axial DWI; the lesion shows diffusion restriction. **C** T1 post-GAD showing minimal postcontrast enhancement. **D** T2* signal intensity time curve: the lesion is hypo-perfused in comparison to the contralateral NAWM with rCBV measuring 1.2 suggesting radiation necrosis (lesion: solid yellow line, NAWM: dashed purple line). **E** MRS showing a neoplastic curve (Cho/Cr = 4.5 and Cho/NAA = 7.25) with the presence of lactate peak. **F** Diffusion kurtosis image showing high mean MK = 661 indicating tumoral recurrence. The patient was on temozolomide which is an anti-angiogenesis chemotherapeutic agent; so, the lesion was hypo-perfused in DSC, yet the MK wasn't affected and showed high value. The final diagnosis was by serial follow-up confirming the diagnosis of recurrence

Abbreviations

MRI	Magnetic resonance imaging
DSC	Dynamic susceptibility contrast
MK	Mean kurtosis
ADC	Apparent diffusion coefficient
RIN	Radiation-induced necrosis
DWI	Diffusion-weighted imaging
DKI	Diffusion kurtosis imaging
MD	Mean-corrected apparent diffusion coefficient
MRS	Magnetic resonance spectroscopy
FOV	Field of view
CBV	Cerebral blood volume
RANO	Response assessment in neuro-oncology
ROI	Region of interest
NAA	N-acetyl aspartate
Cho	Choline
Cr	Creatine
Lac	Lactate
rMD	Relative mean diffusivity
Psp	Pseudo-progression
rKA	Relative axial kurtosis
rMTT	Relative mean transit time
NAWM	Normal-appearing white matter

Acknowledgements
Not applicable.

Author contributions
RA participated in data collection, image interpretations, statistical analysis, writing and editing manuscript. AB, YM and AF participated in the design of study, data collection, image interpretation and statistical analysis. MR participated in image interpretation and supervision. All authors read and approved the final manuscript.

Funding
The authors did not receive support from any organization for the submitted work.

Availability of data and materials
The datasets used and/or analyzed during the current study are available from the corresponding author on reasonable request.

Declarations

Ethics approval and consent to participate
All procedures performed in studies involving human participants were in accordance with the ethical standards of the institutional and/or national research committee and with the 1964 Helsinki Declaration and its later amendments or comparable ethical standards. The study was approved by the Bioethics Committee of the Medical University of Alexandria.

Consent for publication
Informed consent was obtained from all individual participants included in the study.

Competing interests
The authors declare no competing interests.

Received: 2 May 2024 Accepted: 12 July 2024
Published online: 30 July 2024

References

1. Anand T, Ishaque A, Ta D et al (2023) Characterization of white matter alterations using diffusion kurtosis imaging in patients with amyotrophic lateral sclerosis. Brain Behav 13:e3102. https://doi.org/10.1002/brb3.3102
2. Rosenkrantz AB, Padhani AR, Chenevert TL et al (2015) Body diffusion kurtosis imaging: basic principles, applications, and considerations for clinical practice. J Magn Reson Imaging 42:1190–1202. https://doi.org/10.1002/jmri.24985
3. Wang G-Z, Guo L-F, Gao G-H et al (2020) Magnetic resonance diffusion kurtosis imaging versus diffusion-weighted imaging in evaluating the pathological grade of hepatocellular carcinoma. Cancer Manag Res 12:5147–5158. https://doi.org/10.2147/CMAR.S254371
4. Nafe R, Porto L, Samp P-F et al (2023) Adult-type and pediatric-type diffuse gliomas: what the neuroradiologist should know. Clin Neuroradiol 33:611–624. https://doi.org/10.1007/s00062-023-01277-z
5. Ion-Mărgineanu A, Van Cauter S, Sima DM et al (2016) Classifying glioblastoma multiforme follow-up progressive vs. responsive forms using multi-parametric MRI features. Front Neurosci 10:615. https://doi.org/10.3389/fnins.2016.00615
6. Wu X-F, Liang X, Wang X-C et al (2021) Differentiating high-grade glioma recurrence from pseudoprogression: comparing diffusion kurtosis imaging and diffusion tensor imaging. Eur J Radiol 135:109445. https://doi.org/10.1016/j.ejrad.2020.109445
7. Hui ES, Fieremans E, Jensen JH et al (2012) Stroke assessment with diffusional kurtosis imaging. Stroke 43:2968–2973. https://doi.org/10.1161/STROKEAHA.112.657742
8. Law M, Yang S, Wang H et al (2003) Glioma grading: sensitivity, specificity, and predictive values of perfusion MR imaging and proton MR spectroscopic imaging compared with conventional MR imaging. AJNR Am J Neuroradiol 24:1989–1998
9. Nierobisch N, Ludovichetti R, Kadali K et al (2023) Comparison of clinically available dynamic susceptibility contrast post processing software to differentiate progression from pseudoprogression in post-treatment high grade glioma. Eur J Radiol 167:111076. https://doi.org/10.1016/j.ejrad.2023.111076
10. Rafique Z, Awan MW, Iqbal S et al (2022) Diagnostic accuracy of magnetic resonance spectroscopy in predicting the grade of glioma keeping histopathology as the gold standard. Cureus 14:e22056. https://doi.org/10.7759/cureus.22056
11. Sundgren PC (2009) MR spectroscopy in radiation injury. AJNR Am J Neuroradiol 30:1469–1476. https://doi.org/10.3174/ajnr.A1580
12. Pope WB, Hessel C (2011) Response assessment in neuro-oncology criteria: implementation challenges in multicenter neuro-oncology trials. AJNR Am J Neuroradiol 32:794–797. https://doi.org/10.3174/ajnr.A2582
13. Jensen JH, Helpern JA (2010) MRI quantification of non-Gaussian water diffusion by kurtosis analysis. NMR Biomed 23:698–710. https://doi.org/10.1002/nbm.1518
14. Louis DN, Perry A, Reifenberger G et al (2016) The 2016 World Health Organization Classification of Tumors of the Central Nervous System: a summary. Acta Neuropathol 131:803–820. https://doi.org/10.1007/s00401-016-1545-1
15. Abdullah A, El Shitany H, Abbass W et al (2016) Surgical resection of low-grade gliomas in eloquent areas with the guidance of the preoperative functional magnetic resonance imaging and craniometric points. J Neurosci Rural Pract 7:571–576. https://doi.org/10.4103/0976-3147.188629
16. Van Cauter S, Veraart J, Sijbers J et al (2012) Gliomas: diffusion kurtosis MR imaging in grading. Radiology 263:492–501. https://doi.org/10.1148/radiol.12110927
17. Raab P, Hattingen E, Franz K et al (2010) Cerebral gliomas: diffusional kurtosis imaging analysis of microstructural differences. Radiology 254:876–881. https://doi.org/10.1148/radiol.09090819
18. Chuang M-T, Liu Y-S, Tsai Y-S et al (2016) Differentiating radiation-induced necrosis from recurrent brain tumor using MR perfusion and spectroscopy: a meta-analysis. PLoS ONE 11:e0141438. https://doi.org/10.1371/journal.pone.0141438
19. Shi W, Qu C, Wang X et al (2021) Diffusion kurtosis imaging combined with dynamic susceptibility contrast-enhanced MRI in differentiating high-grade glioma recurrence from pseudoprogression. Eur J Radiol 144:109941. https://doi.org/10.1016/j.ejrad.2021.109941
20. Van Cauter S, De Keyzer F, Sima DM et al (2014) Integrating diffusion kurtosis imaging, dynamic susceptibility-weighted contrast-enhanced MRI, and short echo time chemical shift imaging for grading gliomas. Neuro Oncol 16:1010–1021. https://doi.org/10.1093/neuonc/not304

Publisher's Note